Received: 22 October 2024 | Revised: 26 March 2025 | Accepted: 17 June 2025

DOI: 10.1002/esp.70122

RESEARCH ARTICLE

ESPL WILEY

A novel approach for the computation of soil slope stability in distributed hydrologic applications

Riccardo Bonomelli[1] | Marco Pilotti[1] | Luca Piciullo[2]

[1]DICATAM, Università degli Studi di Brescia, Brescia, Italy

[2]Norwegian Geotechnical Institute, NGI, Oslo, Norway

Correspondence
Riccardo Bonomelli, DICATAM, Università degli Studi di Brescia, Brescia, Italy.
Email: riccardo.bonomelli@unibs.it

Funding information
This research was made possible by the following projects: Progetto CNR-IRPI per lo studio sulla dinamica delle colate fangoso-detritiche torrentizie nella Val Rabbia e nel bacino del torrente Blé; RETURN Extended Partnership, funded from the European Union Next-Generation EU (National Recovery and Resilience Plan – NRRP, Mission 4, Component 2, Investment 1.3 – D.D. 1243 2/8/2022, PE0000005).

Abstract

The identification of potential source areas for landslides at the basin scale is a fundamental step for risk assessment in mountain regions. In the literature, many contributions deal with this task by using the Infinite Slope (IS) assumption. However, there is evidence that the widely used IS assumption becomes increasingly inadequate with growing space resolution of the elevation model, contributing to the overprediction of unstable areas that affect this model. In this paper, we propose an original improvement to the stability calculation by presenting a modification of Janbu's method of slices, specifically devised for basin-scale applications. The method is coupled with a hydrological model to provide transient soil saturation during a rainfall event. We show that the proposed improvement is systematically better than the local IS prediction for a set of elementary test cases where a rigorous stability analysis is available, confirming the predictive capabilities of the proposed approach. Finally, we show the applicability of the model at the watershed scale by considering its application to a well-known test case in the literature, i.e. the Mettman Ridge site, Oregon.

KEYWORDS
distributed hydrological modelling, factor of safety, Janbu's method of slices, slope stability

1 | INTRODUCTION

Shallow landslides are a major component of hydraulic hazard in mountain regions and are often triggered by rainfall on steep slopes of a watershed. Soil slope failures are usually triggered by a build-up of porewater pressure during heavy or prolonged rainfalls, undermining the equilibrium between resistance and gravitational forces (e.g. Iverson, 2000). The prediction of the locations which are most susceptible to failure, as well as the amount of material that is destabilized, has great importance for zonation purposes and for designing early-warning systems (e.g. Guzzetti et al., 2020; Piciullo et al., 2018). The interplay between groundwater, water runoff and geotechnical soil properties determines where a soil slope failure will occur; accordingly, hillslope hydrology plays a crucial role in the overall process. To this purpose distributed physically based hydrological models, operating either in steady state or in dynamic conditions (e.g. Baum et al., 2008; Casadei et al., 2003; Dietrich et al., 1992; Dietrich et al., 1993; Dietrich et al., 1995; Iida, 2004), coupled with a soil stability model triggered either by shallow subsurface flow (e.g. Dietrich et al., 2001; Montgomery & Dietrich, 1994) or by a wetting front advancement during rainfall event (e.g. Rosso et al., 2006), have been used to map landslide sources in a watershed. The overall idea is important and attractive: a distributed hydrologic model can provide the surface and shallow subsurface flow paths, derived from the terrain gradient, showing the locations where pore water pressure builds up and where surface runoff is stronger. The first element governs instability, whereas the second is a key variable in the potential evolution of shallow landslides into debris flow. As a consequence, several distributed models at the basin scale have been proposed, based either on actual rainfall-runoff models (e.g. Baum et al., 2008) or on more simplified GIS coupling between land topography and rainfall potential (e.g. Dolojan et al., 2021). It is interesting to observe that since the very first distributed attempt to model soil stability in a watershed (e.g. Haefeli, 1948), the Infinite Slope approach (IS in the following) has been mainly used (e.g. Medina et al., 2021; Murgia et al., 2022; Rossi et al., 2013; Sannino et al., 2024). In their seminal

contribution, Montgomery & Dietrich (1994) developed a distributed model able to combine digital elevation data with near-surface throughflow under steady rainfall and IS stability models. Following a similar idea, the Transient Rainfall Infiltration Grid-based Regional Slope Stability (TRIGRS) model (Baum et al., 2008) computes slope stability considering the transient pore-pressure due to rainfall infiltration. The TRIGRS model is based on an extension of the linearized solution of the Richards' equation (Iverson, 2000), while the IS hypothesis is adopted for slope stability computation. The Shallow Landslides Instability Prediction (SLIP) model (Montrasio et al., 2011) considers the stability conditions of a slope, the soil characteristics and the incoming rainfall, by neglecting the surface run-off and transient infiltration, on the assumption that the entire amount of rain at a certain time instantaneously infiltrates into the soil. Cho & Lee (2002) and Cho (2017) proposed a similar model which uses the Green and Ampt equations (1911) for rainfall infiltration and the IS hypothesis for slope stability. Multidimensional stability models at the watershed scale are an active topic of research (e.g. Burroughs, 1985; Dietrich et al., 2008; Hovland, 1977). Such models usually apply a limit-equilibrium approach to an assumed failure surface, modelling the soil as a collection of rigid blocks. Even though these models require the same input parameters as IS models, they avoid the a-priori definition of a failure surface. However, their application is hindered by the need for an efficient search algorithm to test multiple failure shapes whose number grows exponentially with the number of grid cells used, so the computational burden of this approach may soon become heavy (Dietrich et al., 2008). For these reasons, some constraints must be introduced in order to reduce the computational complexity of the problem (Bellugi et al., 2015). Montgomery et al. (2000) used a predefined rectangular landslide shape with a fixed size; Gabet & Dunne (2002) and Casadei et al. (2003) assumed that the areas of instability have a fixed length-to-width ratio. Okimura (1994) assumed landslides to be rectangular but characterized by a single length-to-width ratio: the size of the landslide is determined by computing the least stable cell using an IS model, then exploring a fixed number of potential rectangular slide masses that include the least stable cell. Qiu et al. (2007) and Oguz et al. (2022) instead explored the three-dimensional stability of ellipsoidal surfaces, using the procedure described by Hovland (1977), neglecting the resisting contribution provided by the roots on the margin of the unstable block. In order to reduce the computational complexity, Lehmann & Or (2012) proposed a different approach in which the shape of the landslide can be general but requires the landslides to originate at a single cell. In their contribution, the hillslope is modelled as different soil columns interconnected by frictional and tensional mechanical bonds represented as fibre bundles. If a certain failure criterion measured on the forces acting at the base of the soil column is met, then its load is redistributed to its neighbours via the aforementioned fibres, which can fail as well, allowing an accurate description of the failure mechanism. Despite the possibility to predict rather general failure shapes, this approach is computationally very intensive and tends to overpredict the number and volume of the landslides. SCOOPS (Reid et al., 2015) extends the 3D Bishop's limit equilibrium analysis (Bishop, 1955) by computing the factor of safety of failure surfaces obtained by the intersection of a sphere of a given radius with the DEM (Digital Elevation Model). In spite of the remarkable contributions listed above, over the last decades, in the modelling of soil stability and transient hydrology at the watershed scale, there is a tendency to keep using the IS model for the computation of stability. According to this approach, the stability is computed at a local scale, neglecting the interaction with the surrounding blocks. However, there is evidence that when the typical vertical scale of the soil depth, h, is comparable to the horizontal scale of the block, Δx, the confining role of the surrounding blocks can be dominant. According to Griffiths et al. (2011), when the $\Delta x/h$ ratio is smaller than 16, the adequacy of the infinite slope assumption is questionable. The practical relevance of this issue was negligible until a few decades ago, when the space resolution of the raster digital elevation models used in the hydrologic applications was relatively coarse, and a typical cell dimension was in the order of 10–20 m. At this scale, considering a reference soil depth typically in the order of 1 m (e.g. Lehmann & Or, 2012), the $\Delta x/h$ ratio was sufficiently large to make the infinite slope approach acceptable. On the other hand, it is now customary to have distributed hydrologic models with Δx in the order of a few meters. This is an important advancement (e.g. Claessens et al., 2005) because a better topographic resolution provides a careful reproduction of the flow paths, which is fundamental for the correct detection of flow accumulation zones and for the physical meaningfulness of the local parameters derived from the pre-processing of the drainage network (e.g. Pilotti et al., 1996) or from local soil properties. In these situations, the scope of validity of the IS assumption is narrowing, because collaborative actions between blocks can become dominant: an unstable block could be sustained by the surrounding ones, or a stable block can be destabilized due to the instability of the upper blocks along the hillslope. Obviously, these situations are considered by traditional geotechnical stability analysis, which studies the stability of the whole slope with methods of increasing complexity (e.g. from Limit Equilibrium Methods to Finite Elements) that, however, are still difficult to implement within a transient hydrologic simulation. In order to provide a solution to these limitations, in this paper we propose an improvement based on a modification of the well-known 2D Janbu's method (Janbu, 1973; U..S Army Corps of Engineers, 2003) as a reasonable compromise between the simplicity of the IS model and the more rigorous complete limit equilibrium methods. Janbu's method considers the collaborative action between consecutive cells along a hillslope and satisfies all equilibrium equations for the whole slope in its complete formulation (Morgenstern & Price, 1965). Even though 3D extensions of the Janbu's method have already been published (Hungr et al., 1989; Qi et al., 2021) a sufficiently simple and computationally unexpensive implementation within a distributed hydrological model at catchment scale is still missing and is hindered by the lack of an efficient search for critical surfaces that may occur in the catchment. In the following, considering that real watershed test cases are inevitably affected by large uncertainties on the actual distribution of soil parameters, we first apply the method to an idealized test case where everything is known, using SLOPE/W module of the GeoStudio software (GeoStudio reference manual, 2021) as a validation tool, showing a systematic improvement with respect to the IS model. Finally, we validate the proposed methodology in terms of landslide susceptibility at the basin scale, using a dataset provided by Bellugi et al. (2015) for a catchment located in Oregon. In conclusion, the main novelties of our contribution are the following:

- Original improvement and implementation of Janbu's method of slices, to make it suitable for catchment scale applications.
- Reduction of computational costs associated to the stability analysis thanks to a novel linearization of Janbu's nonlinear equation.
- Evidence through simple test cases of the superiority of the proposed Janbu's method over the widely used Infinite Slope model, using the same input parameters.
- Implementation at the catchment scale of the proposed Janbu's model inside a state-of-the-art hydrological model able to describe infiltration and runoff processes.

2 | STUDY AREA AND METHODS

In the following, we present the study area of the Mettman Ridge, Oregon together with the methodology used to perform a slope stability analysis. For this purpose, the Infinite Slope model and the novel progressive implementation of Janbu's model are briefly presented. Considering that the application of a slope stability model to a real watershed case is intrinsically dependent on the transient soil saturation caused by the incoming rainfall, we present the implementation of a hydrological model to be coupled with the slope stability one.

2.1 | Study area

We present the application and the comparison of the soil slope stability models to a study area which has been widely discussed in the literature: the Mettman Ridge case, Oregon (e.g. Bellugi et al., 2015; Dietrich et al., 2001; Montgomery & Dietrich, 1994; Rosso et al., 2006). The Mettman Ridge study site (see Figure 1) is located about 15 *km* north of Coos Bay, Oregon, with an area of 0.5 km^2 and consists of steep, highly dissected soil-mantled hillslopes with narrow ridges and steep channels (Bellugi et al., 2015).

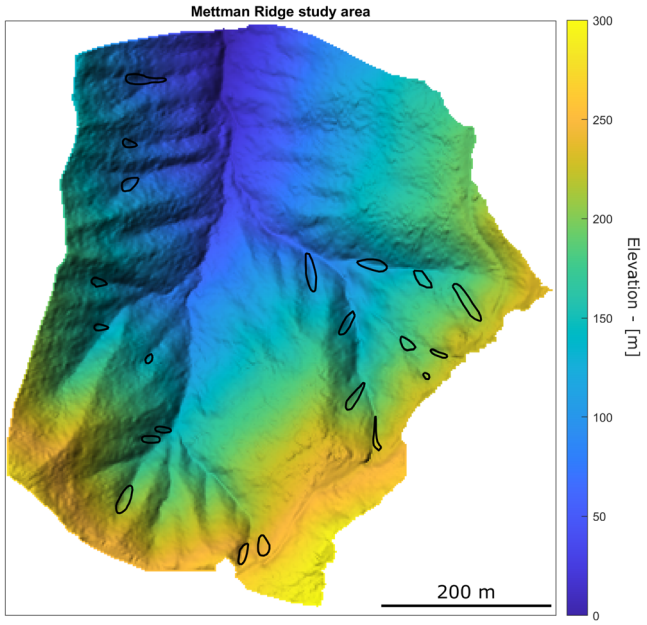

FIGURE 1 Elevation data of the Coos Bay, OR, study site. The solid black polygons represent the mapped landslides that occurred over a 10 year period (Montgomery et al., 2000).

Soil thickness ranges roughly 0.1 *m* to 0.5 *m* on ridges to greater than 2 *m* in topographic hollows (Bellugi et al., 2015). Bedrock outcrops in most areas where the local slope exceeds 45° (Montgomery & Dietrich, 1994), while the colluvium has a friction angle of about 40° and is essentially cohesionless (Bellugi et al., 2015). Roots provide an apparent cohesion via root fibre reinforcement (root cohesion), favouring slope stabilization in shallow soils. Shallow debris flows periodically deliver the colluvial soils to the downstream channel system and scour the bedrock, creating the channel network (Bellugi et al., 2015). Repeated field mapping of the catchment provides, on one hand, a landslide inventory that occurred over a 10 year period (Montgomery et al., 2000) and on the other, field measurements of physical parameters such as hydrological conditions, soil depth and root strength. The data regarding basin elevation, soil depth, root cohesion (basal and lateral) and geotechnical properties of the soil were available from the online repository of Bellugi et al. (2015, 2021). As crucial information to validate a model that must predict soil stability in a catchment, an inventory of landslides that occurred over 10 years is also available (Montgomery et al., 2000). Considering that the high level of uncertainty in the soil description is the real stumbling block when dealing with real watersheds, the use of this reference test case and of the corresponding dataset provides an independent benchmark for slope stability models.

2.2 | Infinite slope model

The most used criterion to assess the stability of a slope is the computation of the Factor of Safety (*FS* in the following), i.e. the ratio between stabilizing and destabilizing forces. A slope characterized by $FS > 1$ is stable, indicating that it is able to withstand the stresses necessary to maintain equilibrium, while if $FS \leq 1$, the slope is unstable and failure may occur if the stressing conditions persist. The IS model (Haefeli, 1948; Skempton & DeLory, 1957; Taylor, 1948) assumes an infinitely long slope, characterized by a sliding failure that occurs along a plane parallel to the surface of the slope. The factor of safety (see also Figure S1.1 of the supporting information) can be written as:

$$FS = \frac{c' + (\gamma_s h - \gamma_w r)\cos^2\beta \tan\phi'}{h\gamma_s \sin\beta\cos\beta}$$
$$\gamma_s = [\gamma_d (h - r) + \gamma_{sat} r]/h \quad (1)$$

where $c'\,[N/m^2]$ is the basal effective soil cohesion, $\gamma_s\,[N/m^3]$ is the vertically averaged soil specific weight of the soil, $\gamma_d\,[N/m^3]$ is the specific weight of dry soil, $\gamma_{sat}\,[N/m^3]$ is the saturated specific weight of the soil, $\gamma_w\,[N/m^3]$ is the water specific weight, $h\,[m]$ is the soil depth, $r\,[m]$ is the water table height measured starting from the potential failure surface, $\beta\,[^\circ]$ is the inclination angle of the slope and $\phi'\,[^\circ]$ is the effective friction angle. It is important to observe that only the equilibrium in the direction orthogonal to the sliding plane is satisfied in the IS model, whereas the equilibrium along the sliding plane is simplified, neglecting the forces that can be transmitted along the boundaries between the considered block and the upper, lower and lateral ones. These simplifications lead either to an underestimate or an overestimate of the equilibrium. Actually, even neglecting the soil resistance to traction, a single block *A* in incipient collapse is constrained by a stabilizing force *F* exerted by the block downslope, *B*. In

this case, the value of *FS* would be underestimated. However, when computing the *FS* of the downslope block *B*, one is neglecting the reaction to *F* exerted by *A*, that now has a destabilizing role. In this case, *FS* could be overestimated. However, the IS model has been extensively applied in literature, often coupled to hydrological models (e.g. Montgomery & Dietrich, 1994; Rosso et al., 2006) that provide the space and time distribution of soil saturation or to more simplified GIS-based analysis in catchment-scale applications (Dolojan et al., 2021; Xie et al., 2004). More recently, the actual scope of the IS applicability has been questioned. Griffiths et al. (2011) performed stability analysis on slopes with different lengths using the Finite Element Method (FEM in the following), and found that the IS model is accurate only for slopes characterized by a length over depth ratio $\Delta x/h > 16$. As the ratio diminishes the IS predictions deviate significantly from the values provided by the FEM method: e.g. for $\Delta x/h \approx 2$ the IS model returns a slope which is half as stable with respect to the predictions of the FEM under the same conditions (Griffiths et al., 2011; Milledge et al., 2012). This deviation is further enhanced if one also considers the role of cohesion. However, due to its simplicity, the IS model is still widely used in catchment scale applications, even in the presence of $\Delta x/h$ ratio close or below the reported threshold (e.g. Chae et al., 2015; Xie et al., 2004).

2.3 | Novel progressive slope analysis using Janbu's model

A well-known method for computing slope stability is the one proposed by Janbu (1973). The Janbu's approach is applicable to general non-circular shear surfaces, overcoming a limitation that characterizes other methods available in literature (e.g. the Ordinary Method of Slices, U..S Army Corps of Engineers, 2003; the Bishop method, Bishop, 1955). Another advantage of Janbu's method is that it is simpler than other complete methods, as defined because they satisfy all equilibrium equations for the whole slope (e.g. Morgenstern & Price, 1965; Spencer, 1967), which are computationally too expensive to be applied at catchment scale. Considering a slope discretized into *n* slices, the factor of safety can be expressed as (see the supporting information section S2 and Figures S2.1 and S2.2 for a detailed derivation, along with Figures 2 and 3):

$$FS = \frac{\sum_{i=1}^{n}\left\{c' a_i + \left[N_i(FS) - u_i a_i + k_0(\gamma_s h_i - \gamma_w r_i)h_i \Delta x \cos^2\beta_i\right]\tan\phi' + 2c'_r h_i \Delta x\right\}\cos\beta_i}{\sum_{i=1}^{n} N_i(FS)\sin\beta_i} \tag{2}$$

where $N(FS)$ is given by

$$N_i = \frac{G_i - \frac{\sin\beta_i}{FS}\left[c' a_i - u_i a_i tan\phi' + 2c'_r h_i \Delta x + k_0(\gamma_s h_i - \gamma_w r_i)cos^2\beta_i h_i \Delta x tan\phi'\right]}{cos\beta_i + \frac{tan\phi' sin\beta_i}{FS}} \tag{3}$$

where $a_i\ [m^2]$ is the inclined bottom area of the *i*-th block, $N_i\ [N]$ is the integral of the normal stresses along the shear surface, which is a function of the safety factor *FS*, $k_0\ [-]$ is the lateral earth pressure coefficient at rest and $c'_r\ [Pa]$ is the effective lateral soil cohesion (typically given by the roots present inside the soil). In the so-called *simplified* Janbu's method (Janbu, 1973) the interslice shear forces are assumed to be equal for each slice. Accordingly, the method satisfies both horizontal and vertical equilibrium but not rotational equilibrium. In the following we will use only the *simplified* Janbu's method, omitting therefore in the following the term *simplified*. Equation (2) is the classical implementation of Janbu's method applied to a 2D slice of a slope with two additional contributions (absent from its original formulation), which are important for its extension to the watershed

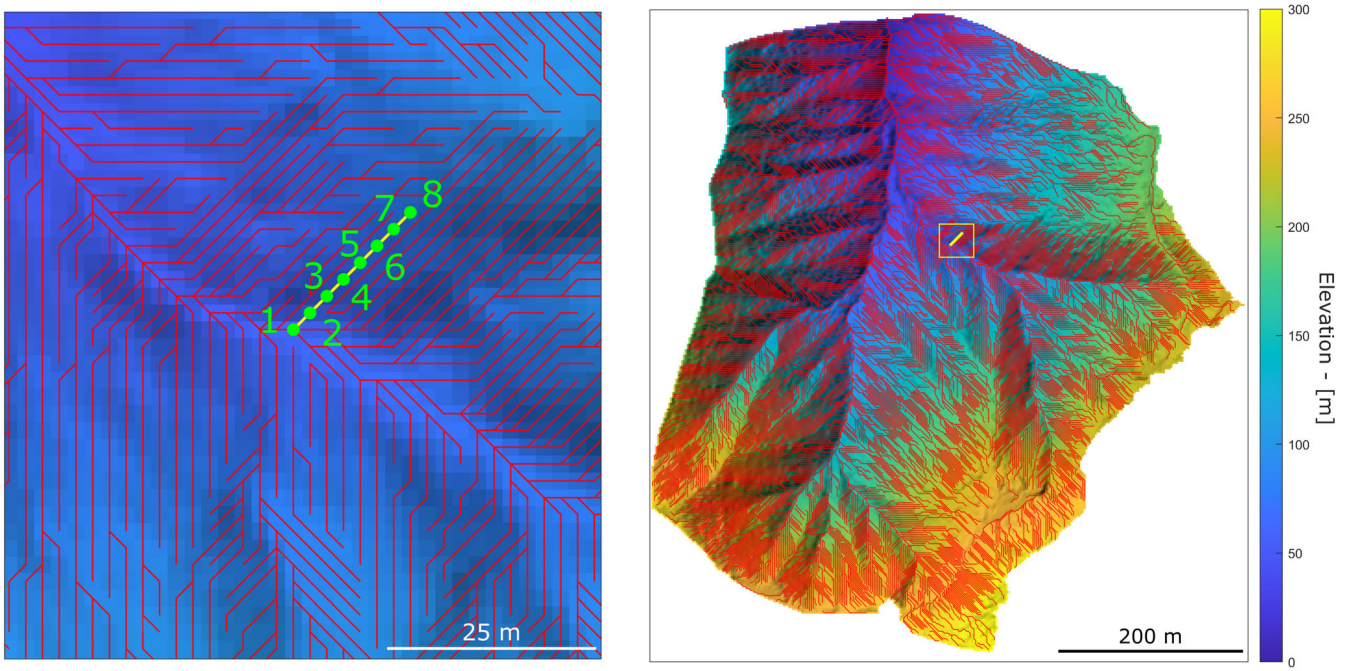

FIGURE 2 (right) Drainage network for a real catchment (Mettman ridge, Oregon); each solid red line represents a slope connecting the DEM cells along the steepest direction. For graphical purposes, slopes draining a small threshold area are not displayed. (left) enlarged view of a single slope of the catchment (shown in yellow on the right): the green dots are the consecutive DEM cells that compose the slope.

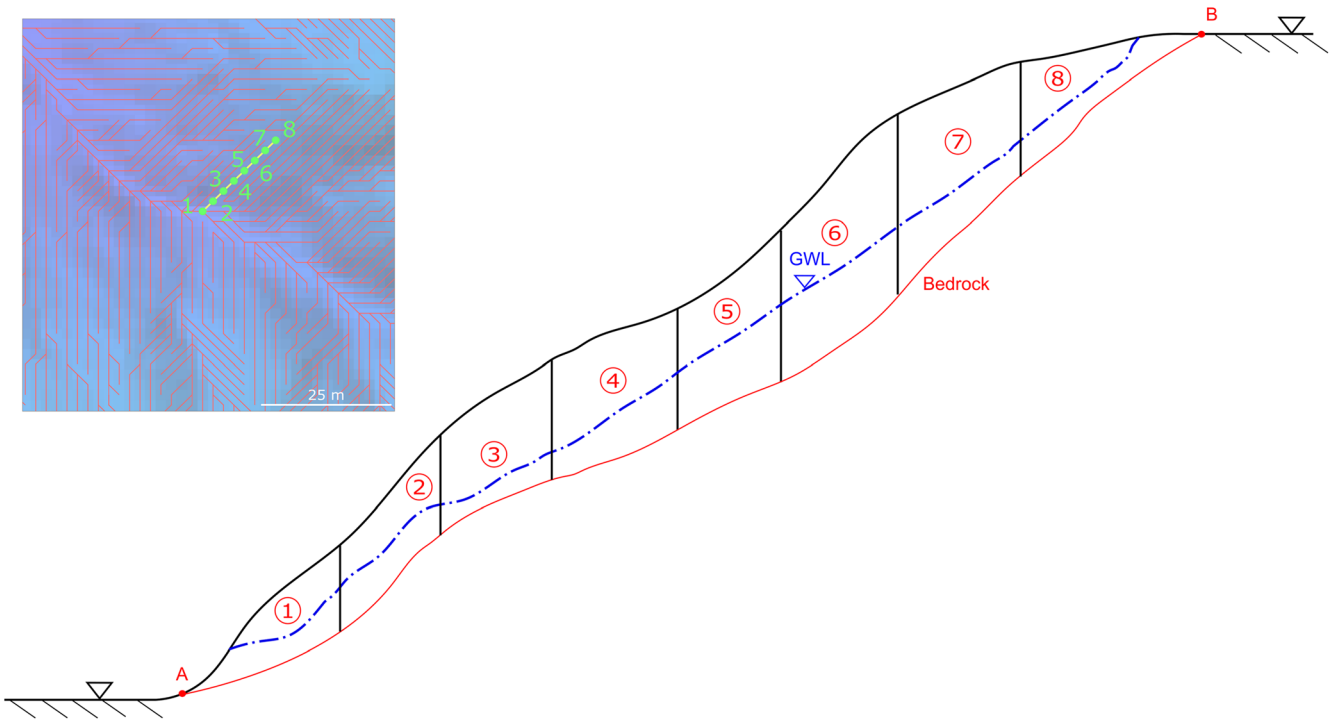

FIGURE 3 Longitudinal section AB of the slope shown in the left panel.

scale (see Figures 2 and 3). These newly introduced contributions arise from the interaction of each slice with the lateral boundary with respect to the sliding direction: the lateral earth pressure, proportional to the k_0 coefficient (e.g. Arellano & Stark, 2000; Burroughs, 1985; Chugh, 2003; Dietrich et al., 2008) and the lateral effective root cohesion c'_r. These contributions arise when considering the slope under investigation to possess an out-of-plane dimension, and therefore, the term "block" or "cell" will now be used instead of "slice". It is important to observe that according to Janbu's method it is possible that one or more blocks, which would be locally unstable (stable) are kept in position (put in motion) by the surrounding blocks, improving the purely local equilibrium of the IS approach. However, Janbu's method was originally devised to test the stability of an entire slope, whose length is set in advance. Let us focus our attention on the stability of the single slope made up by eight cells shown in Figure 2, left panel, and in Figure 3, where the longitudinal section AB of the slope is discretized in blocks with the cell size of the DEM.

In order to find out the length of the subset of AB that is potentially unstable (e.g., 1–2, 1–2-3, 4–5–6-7, …), let us consider block 1 in Figure 3 and let us apply the Janbu's method to the slope made up only by that single block. Using the following notation as a shorthand:

$$\begin{aligned} Num_1 &= \left\{ c'\,a_1 + \left[N_1 - u_1\,a_1 + k_0(\gamma_s h_1 - \gamma_w r_1) h_1\,\Delta x \cos^2\beta_1 \right] \tan\phi' \right. \\ &\quad \left. + 2c'_r h_1 \Delta x \right\} \cos\beta_1 \\ Den_1 &= N_1 \sin\beta_1 \end{aligned} \tag{4}$$

where both Num_1 (Numerator) and Den_1 (Denominator) are functions of the unknown safety factor FS, which is computed using Equation (2) and Equation (3) with $n = 1$:

$$FS_1 = \frac{Num_1(FS_1)}{Den_1(FS_1)} \tag{5}$$

The solution of Equation (5) provides FS_1. Note that at this stage Equation (5) is identical to the IS method when no lateral contribution is present, i.e. $k_0 = 0$ and $c'_r = 0$ (see the supporting information S3 for details). We now consider the slope made up of blocks 1 and 2 and compute the functions Num_1,Num_2 and Den_1,Den_2, to be used into Equation (6) to provide the overall safety factor of the slope made up by the first two blocks, FS_{1+2}:

$$FS_{1+2} = \frac{Num_1(FS_{1+2}) + Num_2(FS_{1+2})}{Den_1(FS_{1+2}) + Den_2(FS_{1+2})} \tag{6}$$

In general terms, the safety factor for the stretch of the slope that goes from the first block to the i-th block can be computed as:

$$FS_{1+\ldots+i} = \frac{\sum_{j=1}^{i} Num_j(FS_{1+\ldots+i})}{\sum_{j=1}^{i} Den_j(FS_{1+\ldots+i})} \tag{7}$$

The upper extent of the unstable part of slope AB is given by the largest value of i (if any) for which $FS_{1+\ldots+i} < 1$. On the other hand, the FS value computed for the entire slope from A to B is precisely Equation (2), i.e. the classical implementation of Janbu's method to the whole slope. At this stage, we introduce a significant simplification: the computation of Equation (2) for the stability of the slope requires solving a polynomial equation for each block along the slope. We argue that this task can be simplified using an approximate novel explicit solution of Equation (2) provided by the following linearization:

$$FS = \frac{\sum_{i=1}^{n} [G_i \tan\phi' + M_i \cos\beta_i + M_i \sin\beta_i \tan\beta_i]}{\sum_{i=1}^{n} [G_i \tan\beta_i]} \tag{8}$$

where M_i is a short-hand notation for $M_i = c'a_i - u_i a_i \tan\phi' + 2c'_r h_i \Delta x + k_0(\gamma_s h_i - \gamma_w r_i) h_i \Delta x \cos^2\beta_i \tan\phi'$ (see the supporting information S4 for the derivation and further evidence on the topic). The newly introduced Equation (8) is crucial to significantly lower the computational times during the slope stability analysis, balancing accuracy and efficiency. Accordingly, one can check every potential failure surface which starts from the toe of the slope (point A of Figure 3) and ends at the n-th block:

$$[FS_1\ FS_{1+2}\ FS_{1+2+3}\ FS_{1+2+3+4}\ \ldots\ FS_{1+2+\ldots+n}] \tag{9}$$

In reality, this is only a subset of the possible failure surfaces that may be present in the slope depicted in Figure 3. As an example, the procedure described does not check the stability of the failure surface located between blocks 3 and 5 (e.g. FS_{3+4+5}). To address this issue we propose to check every consecutive partition of the slope AB while applying the method, in order to explore every location which may become unstable along the slope. So, after computing every *FS* starting from A, one can repeat the procedure described, excluding the first block (therefore starting from the second block) and computing every *FS* up the slope crest. Accordingly, a row is added to the vector (9) of *FS*:

$$\begin{bmatrix} FS_1 & FS_{1+2} & FS_{1+2+3} & FS_{1+2+3+4} & \ldots & FS_{1+2+\ldots+n} \\ & FS_2 & FS_{2+3} & FS_{2+3+4} & \ldots & FS_{2+3+\ldots+n} \end{bmatrix} \tag{10}$$

Eventually, after repeating the previous procedure until only the last block remains, the upper triangular matrix (11) is obtained:

$$\begin{bmatrix} FS_1 & FS_{1+2} & FS_{1+2+3} & FS_{1+2+3+4} & \ldots & FS_{1+2+\ldots+n} \\ & FS_2 & FS_{2+3} & FS_{2+3+4} & \ldots & FS_{2+3+\ldots+n} \\ & & FS_3 & FS_{3+4} & \ldots & FS_{3+4+\ldots+n} \\ & & & FS_4 & \ldots & FS_{4+5+\ldots+n} \\ & & & & \ddots & \vdots \\ & & & & & FS_n \end{bmatrix} \tag{11}$$

The matrix (11) contains all possible *FS* of the partitioned slope. Note that for a slope made of n blocks, the number of consecutive partitions in (11) is a triangular number, given by:

$$N^{\circ}\ of\ checks = \frac{n(n+1)}{2} \tag{12}$$

Within each i-th row in (11), the value of the (i,j) cell indicates the overall *FS* for the failure surface which spans from the i-th block to the j-th block. On the other hand, the *FS* for the i-th block can only be obtained considering the minimum *FS* of all the slopes or sub-slopes (i.e., a collection of consecutive blocks) that contain the i-th block. This value can be computed by applying the following steps:

1. Apply the proposed Janbu's method to the slope under study and compute matrix (11).
2. If at any point along the slope (block k, for instance), a $FS_{1+2+\ldots+k} < FS_{1+2+\ldots+k-1}$ is computed, then all *FS* values before it on the row (i.e. $FS_1, FS_{1+2}, FS_{1+2+\ldots+k-1}$) are updated to the newly computed value $FS_{1+2+\ldots+k}$. After this step, along each row of matrix (11), the *FS* values can never decrease.
3. Repeat step 2 for every row of matrix (11).
4. Finally, the actual *FS* value at a given block along the slope can be obtained by taking the minimum value along each column of matrix (11).

In the following, the matrix obtained by application of the described steps to matrix (11) will be called Janbu's matrix, which is regarded as a novel extension to the classical Janbu's method in terms of the computation of the stability of the slope. It is interesting to note that the diagonal terms of matrix (11) are the *FS* values considering just a single block, which, when the lateral contribution is neglected, are identical to the *FS* computed using the IS model. Due to the limitations intrinsic to the IS model, when the $\Delta x/h$ is too low in the following we suggest to neglect the main diagonal of matrix (11). Having assessed the stability of a single slope, it is possible to extend the described methodology to an entire catchment made by multiple slopes. The subdivision of the whole catchment into slopes is performed by joining the cells of the DEM along the steepest direction (e.g., Pilotti et al., 1996) using the algorithms included in the Matlab-based TopoToolBox software (Schwanghart & Kuhn, 2010). Figure 2 is a visualization example of the output of this analysis. It may occur that the steepest direction changes between the blocks, i.e. when the slope abruptly changes direction or joins another slope in a node (see Figure 2), whenever such a discontinuity occurs, the slope is treated as a separate one (see the supporting information S6 and Figures S6.1 and S6.2 for details).

2.4 | Hydrological model

In order to identify the potentially unstable areas at the basin scale during a rainfall event, a distributed hydrological model must be used which incorporates a stability model. The hydrological model should provide the transient soil saturation at each cell in the basin, to be used in the stability model, as well as the shallow subsurface flow and surface runoff. In the following, we use a proprietary 2D distributed hydrological model (Pilotti & Rosso, 1990), whose operating scheme is the same used in Pilotti et al. (2019). Under the simplified but reasonable hypothesis that the motion of water on the surface of the basin is only controlled by gravity, we could visualize the path followed by rainfall falling on the DEM of the basin (Figure 4a) by computing the directions of steepest descent on its surface. This provides a drainage network that covers every cell of the DEM down to the basin outlet and that, accordingly, is called Space Filling Drainage Network (SFDN, see also Pilotti et al., 1996 and Figure 4b). Where the paths converge and the surface runoff becomes channelled, the SFDN is called a Channel Network (CN, see Figure 4c). Accordingly, the CN is a subset of the SFDN, and these two networks represent the pathlines followed by water flowing first on the hillslopes and then in the channels of the basin. Using the DEM of the basin, the hydrological model first automatically computes its SFDN and then, by using suitable filtering algorithms, the CN (see Figure 4). By moving along these networks, on each cell the hydrological model reads the rainfall falling at time t and computes a suitable water balance that provides the discharge flowing to the downstream cell, and, eventually, to the basin outlet (see Figure 4, red dot).

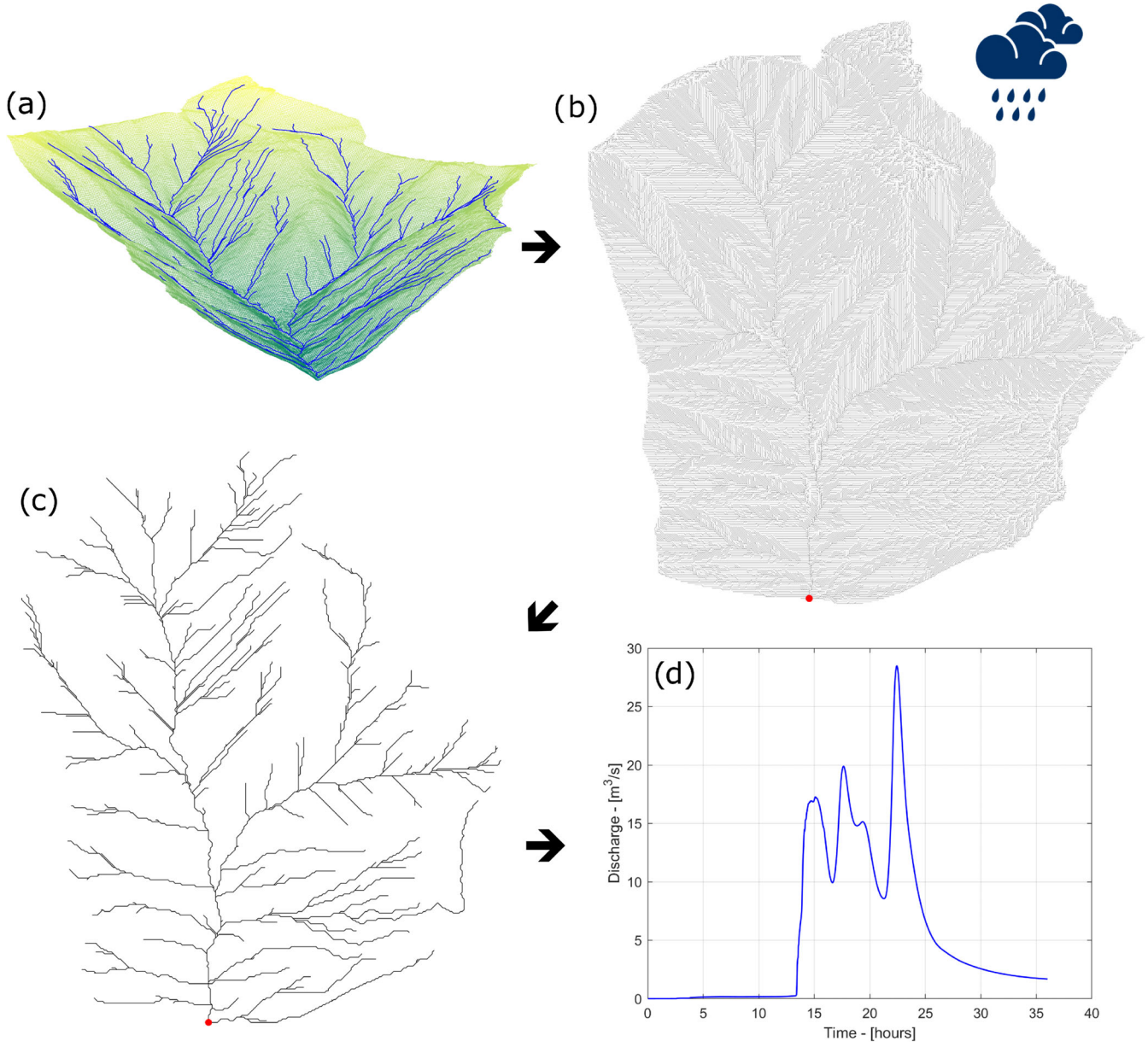

FIGURE 4 (a) DEM of a watershed, from which (b) the space filling drainage network (SFDN) and (c) the channel network (CN) are computed with suitable filtering algorithms. Each cell of the watershed is linked along the SFDN and the CN. At the connections between the SFDN and CN, the runoff is conveyed within the CN. (c) Water is transferred from rainfall to discharge at the basin outlet, moving along the SFDN and CN of the DEM of a watershed. The red dot in (b) and (c) is the basin outlet.

Figure 5 shows the hydrological processes that are computed within each cell of the SFDN. Each cell has a two-storage structure, and for each storage, a local water balance is computed that provides the temporal evolution, during the flood event, of the state variables in the cell:

$$\frac{dW_j}{dt} = R_j + Q_{j,u} - Q_{j,d} \qquad j = 1,2 \tag{13}$$

where the subscript $j = 1$ refers to the surface runoff storage and $j = 2$ to the subsurface flow, $W_j\ [m^3]$ is the volume of water available inside the storage, function of the water depth (h_r or h_g in Figure 5), $Q_{j,u}\ [m^3/s]$ is the flow rate entering the reservoir from the cells located upstream along the SFDN, $R_j\ [m^3/s]$ is the precipitation on the cell, net if $j = 1$ and infiltrated if $j = 2$. Finally, the discharge flowing out of each storage, $Q_{j,d}\ [m^3/s]$ is linked to the stored water volume W_j according to a power relation

$$Q_{j,d} = k_j W_j^{m_j} \qquad j = 1,2 \tag{14}$$

where the value of the exponent $m_1 = 5/3$, represents absolutely turbulent runoff and $m_2 = 1$ represents saturated Darcy flow, k_j is a dimensional constant to be determined, on the basis of the value of the Strickler coefficient for the surface flow K_s and of the local slope in the cell s, according to the relation

$$k_1 = \frac{K_s\, s^{0.5}}{\Delta x^{2m_j - 1}} \tag{15}$$

where Δx is the width of the DEM cell. If $j = 2$, k_j is computed as

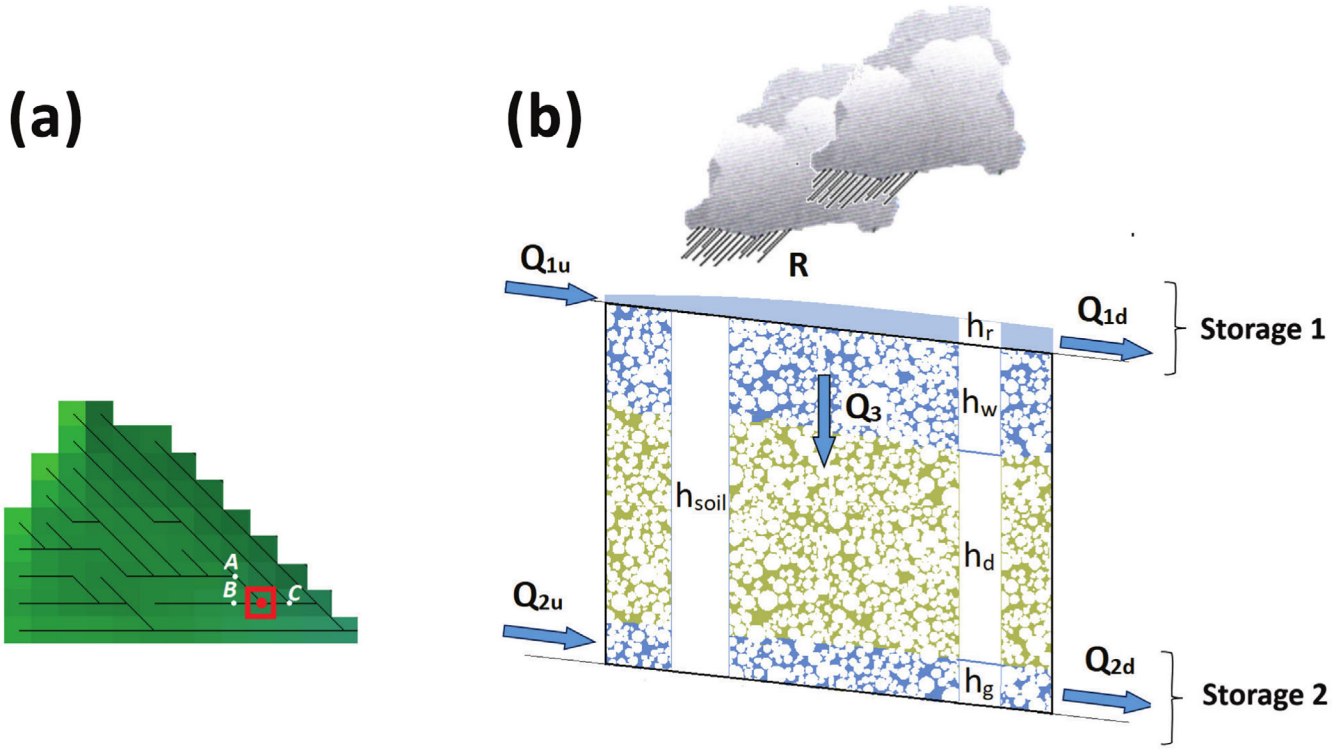

FIGURE 5 Hydrological processes computed within each cell of the space-filling drainage network. The previous block on the right is a vertical-section of the cell framed in red on the left, that receives inflow from cells A and B and feeds cells C. Net rainfall is computed from local rainfall R using the Green-Ampt method. Net rainfall contributes to the water depth h_r of the upper storage, whose balance provides local runoff $Q_{1,d}$ on the basis of incoming runoff $Q_{1,u}$, from upstream cells A and B and of Manning's equation. h_w is the thickness of the saturated layer from above, i.e. the position of the wetting front of the infiltrating rainfall. When $h_w = h_{soil}$, the local soil depth, the wetting front is on the bedrock and a local shallow aquifer parallel to the soil surface is triggered. The local aquifer balance uses $Q_{2,u}$ (different from zero only if a local aquifer is present at cells A or B) and $Q_{2,d}$, that is computed according to Darcy's equation. The balance provides h_g, the thickness of the saturated layer on the bedrock. Considering that a local aquifer can be originated also by Q_{2u}, it can be present in a cell even if $h_w < h_{soil}$. In this case, two saturated layers are locally present, separated by a dry layer $h_d = h_{soil} - (h_w + h_g)$.

$$k_2 = \frac{K_p}{\Delta x} \tag{16}$$

where $K_p\,[m/s]$ represents a permeability coefficient for saturated sub-surface flow in a direction parallel to the slope. Starting from rainfall R_j on the cell, the net rainfall and the infiltration are computed using the Green-Ampt method, which also provides the local wetting front (h_w in Figure 5) within the soil column.

When the flow transferred along the SFDN reaches a cell where the CN is present, the flow enters the riverbed and from there it is transferred to the basin outlet with a Muskingum-Cunge flood routing scheme (Cunge, 1969). To this purpose, the CN is subdivided into stretches whose length is given by the dimension of the cell in the DEM. Along each stretch and at each time step, the unknown downstream flow rate discharge $Q_2(t+\Delta t)$ is computed as a function of the upstream flow rate Q_1 as

$$Q_2(t+\Delta t) = a_1 Q_1(t) + a_2 Q_1(t+\Delta t) + a_3 Q_2(t) \tag{17}$$

where the coefficients are given by

$$a_1 = \frac{\overline{K}X + 0.5\Delta t}{\overline{K}(1-X) + 0.5\Delta t} \quad a_2 = \frac{-\overline{K}X + 0.5\Delta t}{\overline{K}(1-X) + 0.5\Delta t} \quad a_3 = \frac{\overline{K}(1-X) - 0.5\Delta t}{\overline{K}(1-X) + 0.5\Delta t} \tag{18}$$

and where the parameters $\overline{K}$ and X are calculated as a function of the local unit width discharge $q\,[m^2/s]$, of the channel slope s and of the flood wave celerity $c\,[m/s]$ as follows:

$$\overline{K} = \frac{\Delta x}{c} \quad X = 0.5\left(1 - \frac{q}{s\,c\,\Delta x}\right) \tag{19}$$

where in turn the celerity c is computed on the basis of the local average velocity, computed using Manning's equation. A simple example that shows the influence of the slope topography on the dynamics of soil saturation in the hydrologic model is shown in Figure 6 for an elemental hillslope made with a sequence of 28 cells, each with a side of 10 m. Three different elevation profiles have been considered: linear (case A), convex (B) and concave (C). The slope is initially dry with a uniform distribution of soil depth $h_{soil} = 0.4\,m$, porosity $\Phi = 0.3$ and suction $\Psi = 0.19\,m$ and saturated permeability $K_p = 8.3 \cdot 10^{-5}\,m/s$. A steady rainfall of $0.05\,m/h$, lasting three hours, has been assumed. The coloured maps on the right of Figure 6 show the time and space evolution of slope saturation during 20 days after the end of the event, in the three cases of linear, convex and concave slope. Red colour indicates complete saturation which is also the initial condition of the three slopes. In contrast, the violet colour indicates the minimum level of saturation, which is followed by desaturation (white). Whereas for slope A, desaturation proceeds at the same rate from upstream to

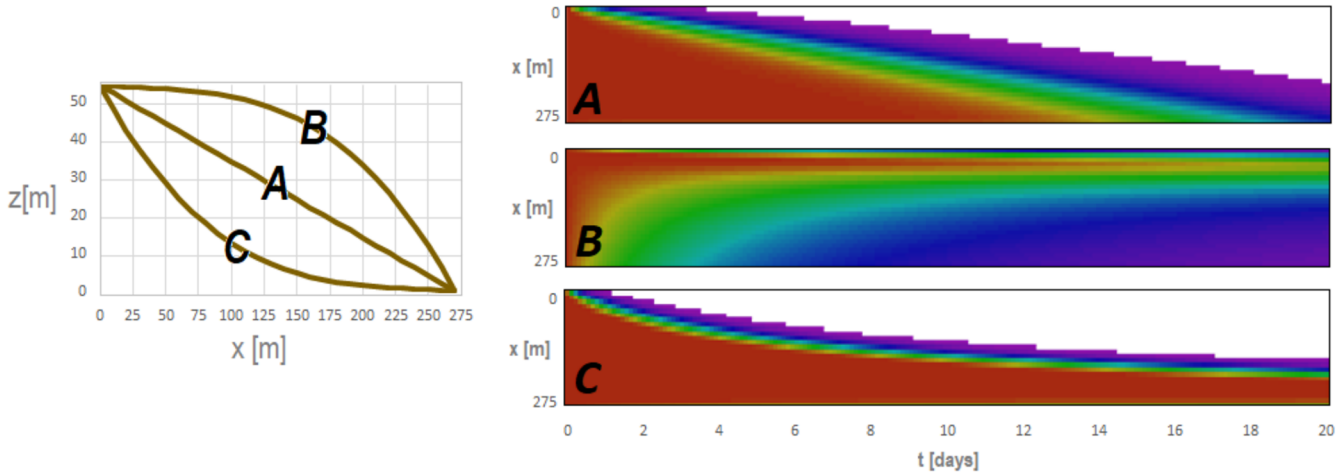

FIGURE 6 Space–time evolution of average soil saturation along three slopes with the profile shown on the left. Along a 20 days long period, the saturation decreases from 1 (red) to 0 (white) with different spatial patterns that reflect drainage and accumulation governed by the local slope.

downstream, this does not happen in the case of the convex slope B. The steepest cells are desaturated more rapidly, and a perching aquifer remains, whose slow desaturation feeds the downstream cells. Finally, in the concave slope, the faster desaturation of the upper part of the basin keeps a prolonged high saturation level at the foothill.

2.5 | Implementation

In this section, we describe the main steps that we followed to perform the slope stability analysis to the described case study. This step-by-step guide will allow the reader to apply the presented methodology for similar case studies.

- Starting from the DEM of the catchment, the entire watershed is divided into slopes following the steepest direction (also called SFDN). Furthermore, a CN must be defined starting from the SFDN using suitable filtering algorithms.
- Distributed soil data (depth, cohesion, friction angle, saturated hydraulic conductivity, …) are assigned to each cell of the DEM. A rainfall event, uniform or spatially variable, must be provided.
- By accomplishing the rainfall-runoff hydrological simulation, the transient soil saturation is computed at each cell of the DEM. Rainfall infiltrates in the soil and propagates along the drainage network according to the physics described in Section 2.4.
- At each time step of the hydrological simulation, the transient soil saturation is used by the progressive Janbu's method to compute the factor of safety of each slope using Janbu's matrix (11).
- The previous computations are repeated for each time step of the hydrological simulation, up to the end of the desired simulation time.
- At the end of the simulation, the minimum *FS* that has occurred is retrieved for each cell of the DEM, thus highlighting the location of the areas that become unstable due to soil saturation.
- If available, a comparison with the observed unstable areas can be performed to assess the quality of the classifier adopted. To achieve this purpose, the Receiver Operating Curves (ROC) (Metz, 1978) can be used on the basis of surveyed landslides. By integrating the areas below a ROC curve, an overall threshold-independent quantitative information about the quality of the binary classifier (stable, unstable) being tested can be obtained. The higher the Area Under the ROC Curve (AUC in the following, whose maximum is 1), the higher the quality of the classifier. According to Davis & Goadrich (2006), ROC curves can present an overly optimistic view of a classifier's performance if there is a large skew in the class distribution. For this reason, Precision-Recall (PR) curves (Manning & Schutze, 1999) may be used in addition to ROC curves, considering the dataset under investigation for a clearer picture.

3 | RESULTS

In the following, the unstable areas are computed for a test slope where every input data is known, comparing the proposed progressive Janbu's method, the IS method and the Morgenstern & Price procedure (1965). An additional test case is also presented in the supporting information S5. The output of Morgenstern & Price procedure is considered as the reference solution, since both the factor of safety and the position of the critical failure surface area provided by this method are very close to the output provided by a FEM analysis performed with the same conditions (Cheng & Lau, 2014). For the sake of simplicity and for a clearer comparison, in the following test case $k_0 = 0$ and $c'_r = 0$. The software GeoStudio (SLOPE/W module, Geostudio reference manual, 2021) has been used to compute the Morgenstern & Price solution, choosing the half-sine function as an inter-slice shear force function, as customary for stability analysis (Cheng & Lau, 2014). All admissible failure surfaces that can arise in a given slope have been dynamically tested, displaying only the ones that are characterized by a factor of safety that is smaller than unity. The considered slope is analysed in fully saturated conditions. Lastly, we show the applicability of the proposed Janbu's method to the study area described in Section 2.1, showing a systematic improvement in terms of the prediction of the unstable areas with respect to the IS model.

Slices	1 – 10	11 – 20
$h - [m]$	1	1
$\beta - [°]$	11	27
$\Delta x - [m]$	5	5
$m - [-]$	1	1
$\gamma_{sat} - [N/m^2]$	19 743	19 743
$c' - [N/m^2]$	2 500	2 500
$\phi' - [°]$	30	30

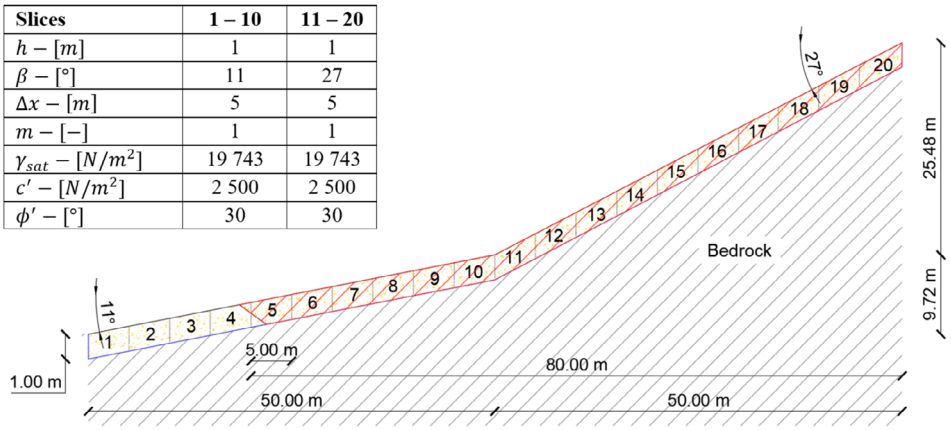

FIGURE 7 Visualization of test case 3.1. The depth of soil along the SLOPE has been enlarged for graphical reasons. The inset on the left shows the geotechnical properties of the soil. h is the soil depth, β is the inclination of the block, Δx is the block length, $m = r/h$ is the normalized free surface height (the slope is completely saturated), γ_{sat} is the saturated unit weight of the soil, c' is the effective cohesion of the soil and ϕ' is the effective friction angle. The red shaded area is the amount of soil that is unstable $(FS \leq 1)$ according to SLOPE/W (GeoStudioreference manual, 2021).

3.1 | Theoretical test case

This test case consists of the idealized slope shown in Figure 7. The slope is equally divided into two parts: the first 50 m stretch has a constant gradient of 11°, while the remaining portion is characterized by a uniform steeper gradient of 27°. The geotechnical characteristics of the soil are shown in Figure 7.

In Figures 7 and 9, the output of SLOPE/W for the test slope is shown. The unstable area as computed by SLOPE/W, spanning from the 20 m station up to the top of the slope, is red-shaded. As can be seen, the instability of the steeper region also affects the upper part of the less steep region. Figure 8a shows the corresponding matrix (11). Figure 8b shows Janbu's matrix: as one can observe, several cells that would be wrongly considered stable based on a purely local analysis of matrix (11) turn out to be unstable due to the destabilizing contribution of the upper cells. For instance, notice how in row 6 of Figure 8a, which corresponds to the shear surface which starts from the 25 m mark going upstream, the slope would be stable up to the second-last cell, as highlighted by the values of the factor of safety. Then, if the contribution of the last cell is considered, the overall slope is no longer stable (see row 6 of Figure 8b) since the factor of safety reported in the last column of row 6 is less than 1 (i.e. $FS_{6+7+\ldots+20} < 1$). This newly computed factor of safety is then assigned to all cells already encountered along the row, flagging them as unstable, according to the procedure discussed in Section 2.3. Figure 9 summarizes the entries of matrix shown in Figure 8b in a single line plot, showing for each column the minimum computed FS using the progressive Janbu's method, together with the results provided by the IS method and the stable and unstable areas by SLOPE/W. Figure 9 shows that, as expected, the IS model is unable to predict unstable cells in the milder stretch since it considers only local contributions, whereas the proposed Janbu's method is able to correctly predict the extension of the failure surface even in the less steep region. Overall, the proposed Janbu's method predicts failure for the last 75 m (93.75% of the overall unstable area), while the IS method only for the last 50 m (62.50%). Moreover, the explicit linearization in Equation (8) provides a maximum error of around 3% with respect to the solution of the nonlinear equation (2), being computationally about 500 times faster for the whole analysis with respect to solving the nonlinear equation (2) at each check, thus proving its effectiveness. In particular, running the analysis for this simple slope took around 6 seconds computing the FS at each partition using the nonlinear equation (2), while just 0.01 seconds using the explicit linearization provided in Equation (8). Finally, the IS model took less than 0.005 seconds to run on this test case. All reported times make reference to a computer having an AMD Ryzen 95900HX 3.30 Hz as a processor. This case is a clear example of the limits of the IS approach in a simple situation which may arise inside any stability analysis at the basin scale. Although in this example we used a small $\Delta x/h$ ratio $5/1 = 5$, the computation of the stability along the less steep part of the slope does not improve when a larger dimension of the cells, up to $50/1 = 50$, is used. Further investigations show that if a larger Δx (up to 25 m) is adopted in the proposed Janbu's method to model this simple slope, the results are still closer to the solution computed by SLOPE/W.

3.2 | Watershed application

The analysis of the synthetical test case has shown the superiority of the proposed method over the IS method in a case where the actual stability of the slope is known. On the other hand, the method is relatively more complex with respect to the IS, which is based on a pure local analysis, and it is important to show its actual applicability at the watershed scale. To this purpose, in the following we present the application of the proposed methodology to the Mettman Ridge test case, already introduced in Section 2.1. Transient soil saturation was obtained using the described hydrological model, considering a rainfall of 100 mm/d lasting 24 hours, as done previously by Rosso et al. (2006). In Figure 10 we compare the results provided by the IS model and by our progressive Janbu's method using the same soil parameters as reported in Bellugi et al. (2015). As one can observe, the IS model correctly predicts all the unstable areas, but with a strong

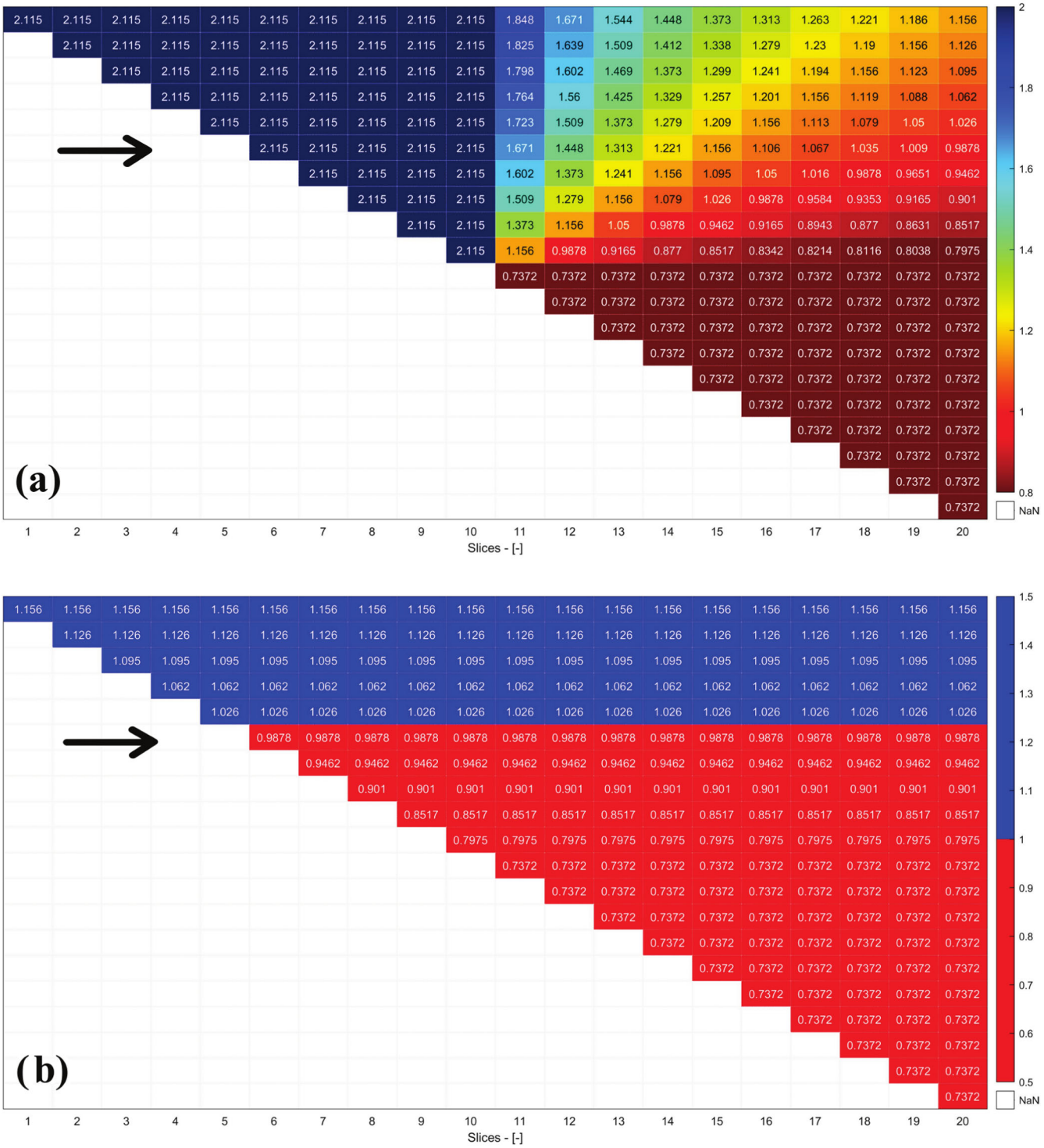

FIGURE 8 Steps for the application of the progressive Janbu's method for the slope in Figure 7: a) matrix (11), b) Janbu's matrix. The arrow points to the line discussed in the text.

tendency to overpredict unstable areas. On the other hand, the proposed Janbu's method fails to predict some unstable areas, but the overprediction is significantly reduced.

The graphs in Figure 11 have been obtained with *FS* varying between 0.4 and 2 with a 0.05 step, using the surveyed landslides shown in Figure 1. Figure 11 confirms that the IS model (AUC = 0.81) performs better with respect to the random classifier (AUC = 0.50), i.e. just assuming a 50% chance that each cell is unstable. On the other hand, Janbu's method proves itself to be a more robust classifier, performing slightly better with respect to the other models (AUC = 0.86). In this case, the hydrological reproduction of 1 hour of real event took around 1 minute of computational time; at each overall check, the IS model computes the stability of every single cell of the catchment in around 0.1 seconds while the proposed Janbu's method takes about 3 seconds when the explicit linearization provided in Equation (8) is used. Despite the modest improvement in terms of the AUC on such a test case, it can be noted that the proposed Janbu's method outperforms the IS model for every possible choice of the *FS* used to distinguish between stable and unstable areas, thus proving its effectiveness.

Considering the highly imbalanced dataset between stable cells, i.e. 71,745 and unstable cells, i.e. 1,074, the use of the ROC curves alone may generate an overly optimistic picture of the quality of the classifiers (Davis & Goadrich, 2006). This may be the case considering the high AUC value of the IS model, considering that most of the cells are classified as unstable, as it can be seen in Figures 10 and 11. For this reason, Figure 12 shows the Precision-Recall curves obtained using the same range of *FS* values used to compute the ROC curves.

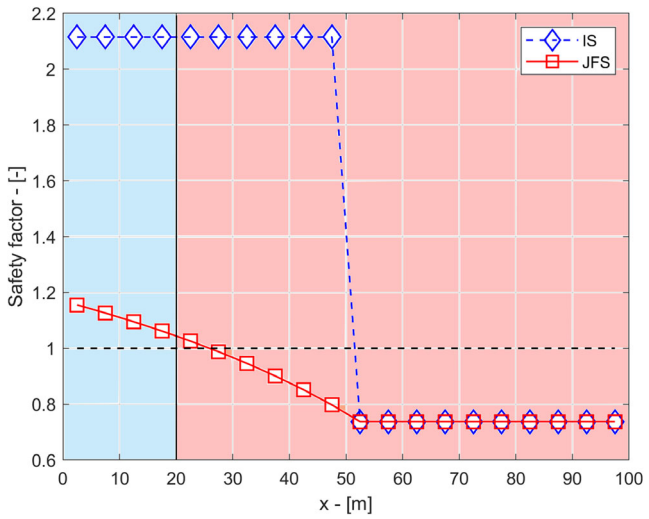

FIGURE 9 *FS* computed using the proposed Janbu's method (JFS) and the infinite slope method (IS) for the slope of Figure 7. The values of JFS are obtained from the matrix shown in Figure 8b by taking the minimum *FS* value along each column. The light blue and red shadings represent the stable and unstable areas computed using SLOPE/W.

As it can be noticed, the AUC even for the PR curves is much higher considering the proposed Janbu's method (0.137) with respect to the IS model (0.071). Both models perform better with respect to the no-skill predictor, obtained by computing the probability that a given cell is unstable, for any Recall value. ROC and PR curves are just two methods to judge the quality of a classifier, and, despite being threshold independent, they may offer a distorted view of the classifier adopted if no other metrics are computed (Chicco & Jurman, 2023). For this reason, in Table 1, other possible metrics are reported, which are computed for both models using a threshold of $FS = 1$ to distinguish between stable and unstable cells. As one can observe, the progressive Janbu's method performs better for most indicators. In particular, the Unstable Area Ratio (given by the ratio between the area of the unstable cells predicted by the model and the area of the observed unstable cells) and the Unstable Volume Ratio (similar to the latter, using volume instead of area), highlight how the proposed Janbu's method is much closer to the theoretical value of 1 with respect to the IS model. Therefore, the IS model overestimates the unstable areas both in terms of areas and volumes. Furthermore, the True Positive Rate considering the IS model is higher with respect to the progressive Janbu's model, meaning that the probability of detection of an unstable area is higher considering the IS model. This is due to the large amount of predicted unstable areas (TP + FP) with respect to the progressive Janbu's model. On the other hand, the probability of false alarm (also known as False Positive Rate) is much lower considering the progressive Janbu's method. This is confirmed by observing that there are fewer cells with respect to the IS flagged as unstable; thus, the probability that one of them is mistakenly flagged as positive is much lower with respect to the IS model, in which the high number of false positives dominates.

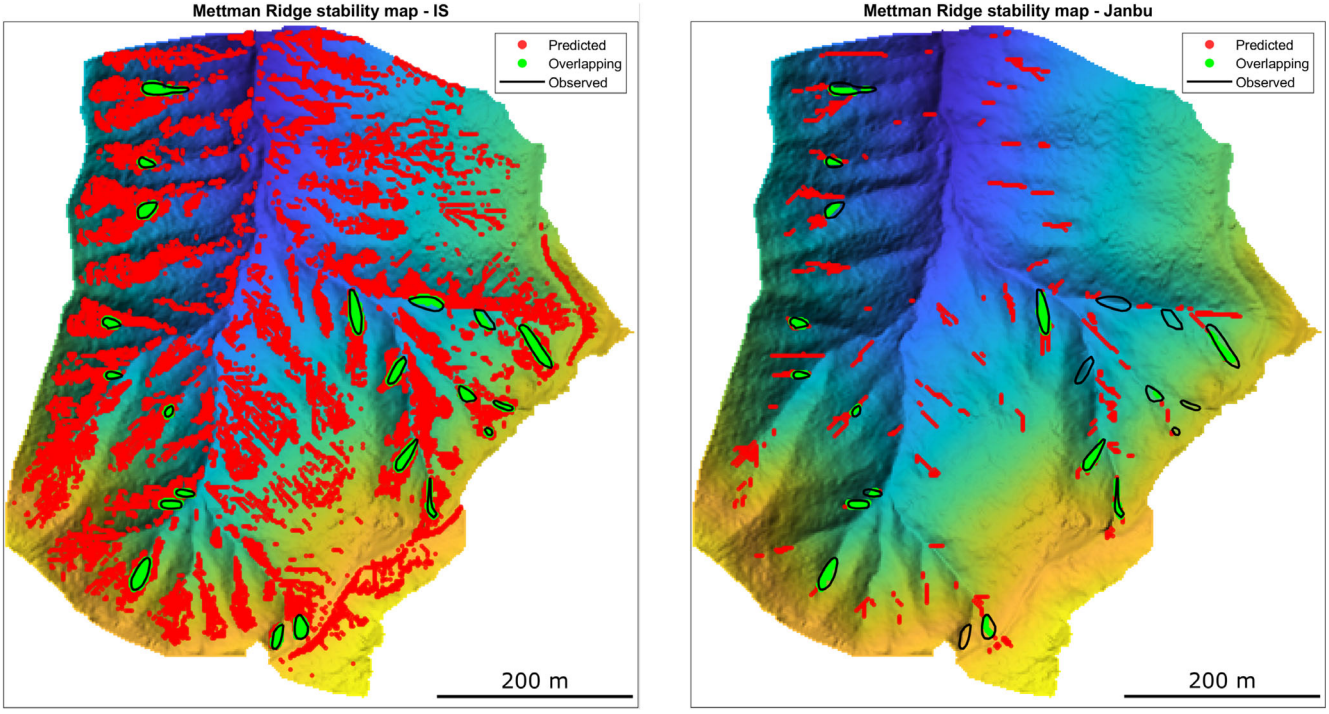

FIGURE 10 Stability map output of the IS model (left) and of the progressive Janbu's method (right). The red dots indicate the false positive (FP) areas, which are unstable areas outside of the observed unstable areas (black polygons). The overlapping between observed and computed unstable areas (true positive, TP) is displayed in green.

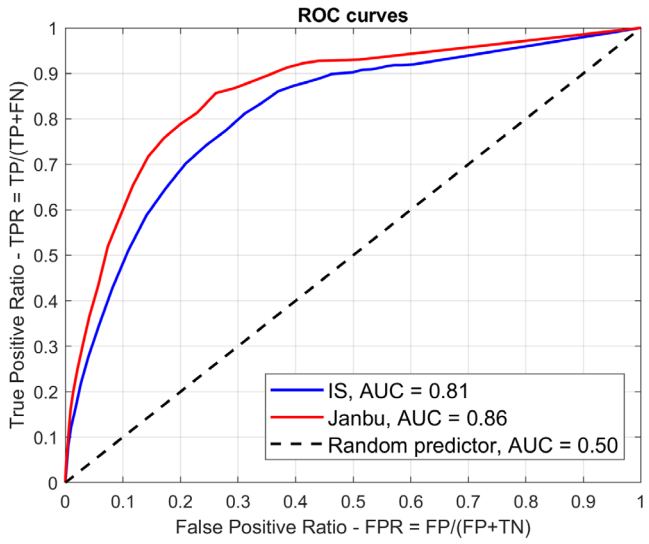

FIGURE 11 Receiver operating curves (ROC) for the IS (showed in blue), the proposed Janbu's method (in red) and the no skill predictor (dashed black line).

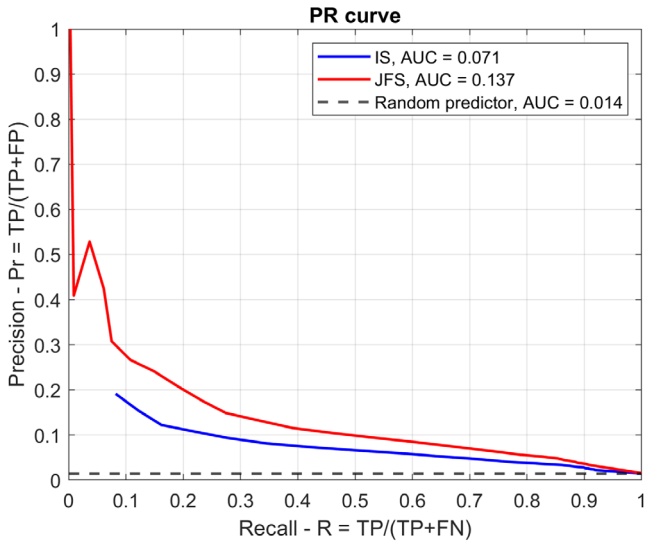

FIGURE 12 Precision recall curves (PR curves) for the IS model (shown in blue) and the proposed Janbu's method (in red). The dashed black line represents the no-skill predictor.

TABLE 1 Computed dimensionless metrics to evaluate the proposed Janbu classifier against the IS model. The observed cumulative unstable area and volume are 4297 m^2 and 6002 m^3 respectively.

	IS	Janbu
TP (True Positives)	753	237
TN (True Negatives)	56,774	70,630
FP (False Positives)	14,971	1,115
FN (False Negatives)	321	837
Unstable Area Ratio	14.63	1.25
Unstable Volume Ratio	11.55	1.35
MCC (Matthews Correlation Coefficient)	0.57	0.59
TPR (True Positive Rate)	0.70	0.22
TNR (True Negative Rate)	0.79	0.98
FNR (False Negative Rate)	0.29	0.77
FPR (False Positive Rate)	0.21	0.01
PPV (Positive Predictive Value)	0.04	0.17
FDR (False Discovery Rate)	0.95	0.82
NPV (Negative Predictive Value)	0.99	0.99
F1 score	0.08	0.19
Accuracy (ACC)	0.79	0.97
BM (Bookmaker Informedness)	0.49	0.20
MK (Markedness)	0.04	0.16
FMI (Fowlkes Mallows Index)	0.18	0.20

4 | DISCUSSION

In order to identify the potentially unstable areas at the watershed scale during a rainfall event, a distributed hydrologic model can provide the transient soil saturation at each site in the watershed, effectively taking into account the role of slope topography on the dynamics of soil saturation. The simple example reported in Figure 6 clearly shows that distributed hydrologic models can provide the topography-controlled transient soil saturation distribution needed to compute stability. Within the limits of the approximations made in reproducing the complex processes involved in soil hydrology and cast within a suitable probabilistic framework to overcome the uncertainties of soil parameter variability, these models could provide the position of potential soil slips within a watershed, in response to specific rainfall events conditioned to the past saturation history of the watershed. In this direction, the use of high-resolution DEMs is key to a better reproduction of local slope, flow propagation directions and soil saturation build-up during rainfall events at the watershed scale. However, if this is the future trend, the widely used IS method will not be a suitable approach because the stability of a cell within a high-resolution DEM cannot be analysed independently from the stability of the surrounding cells, as shown, among others, by Milledge et al. (2012), who found that when the $\Delta x/h$ ratio is smaller than 16, the adequacy of the IS assumption is questionable. The method proposed in this paper for the prediction of unstable areas is an adaptation of the well-known Janbu's method to a space-distributed application and can overcome this limitation. It is a computationally viable compromise between sophisticated approaches for the computation of soil stability (e.g. FEM) and the sheer simplicity of the IS method. The simple test cases, which consider an elemental situation that may occur within a real watershed, have shown the superiority of this method in situations where the actual soil stability is known and where all information about soil and saturation is fixed, thus eliminating the parameter uncertainty typical of real catchments. Finally, the Mettman Ridge case shows that the IS has a dramatic tendency to overpredict unstable areas, a flaw well documented in the literature (e.g., Bellugi et al., 2015). Figure 10 shows that too many cells are classified as unstable by the IS, strongly limiting the usefulness of this model in practical situations. Considering the discretization of the DTM used in the Mettman Ridge case (2 m), and the average soil depth in the basin (0.67 m), a possible reason behind the poor performance of the IS model may be the relatively low $\Delta x/h$ ratio, around 3, well below the

threshold of 16 highlighted by Milledge et al. (2012). Alongside these positive conclusions, one cannot help but observe that, regardless of cases in which the data were measured in an extensive form (e.g., Mettman Ridge), every modelling chain that aims to predict soil instability due to rainfall events is hindered by the problem of estimation of the involved parameters. In this direction, the soil depth distribution, which can only be guessed at the basin scale, has paramount importance since the slope stability method assumes that the failure surface occurs at the discontinuity of permeability between the soil and the bedrock. To address this issue which may impair the use of the model it is possible either to use empirical methods that try to correlate the soil depth with elevation or local slope (Catani et al., 2010), or to use the thickness of the dynamic saturated layer provided by the hydrological model, as reported in Rosso et al. (2006). According to this approach, at each time step of the simulation, the stability of the slopes is verified assuming that the most critical shear surface occurs at the interface between the saturated and unsaturated zone, a key information provided by the implemented hydrological model. Regardless of the way in which the soil depth is computed, a key limitation of the proposed slope stability model (and also of the IS model) is the assumption that the most critical failure surface must pass either at the interface between the soil colluvium and the bedrock (thus requiring a pointwise information about the depth of the soil) or at the interface between the saturated and unsaturated zone (provided by an hydrological model and highly dependent on the saturated hydraulic conductivity). This limitation is absent in other slope stability models, which do not require such a piece of information, but instead rely on an iterative search for the most critical failure surface. An example of such models is SCOOPS3D (Reid et al., 2015), in which the failure surface is obtained by the intersection of a trial sphere with the DEM. To limit the excessive number of surfaces to be tested, usually the approach allows the user to define some search restrictions which may influence the results and computational times. Despite this issue SCOOPS3D is based on the 3D extension of Bishop's method of slices (Bishop, 1955) which is more suitable for rotational failures since on one hand the horizontal equilibrium equation is not satisfied (U.S. Army Corps of Engineers, 2003) and on the other the failure surface must be a sphere (or a circle in 2D), which is usually not the case in shallow landslides. The proposed Janbu's method, instead, by disregarding the rotational equilibrium equation, satisfies the horizontal equilibrium equation, thus being more suitable for shallow landslides. It is important to stress that the standard IS model satisfies vertical equilibrium only, despite its widespread applications. Complete equilibrium methods, i.e. methods that satisfy all equilibrium equations (e.g. FEM or Morgenstern & Price procedure) are still computational inefficient when applied to entire catchments, especially considering the number of failure surfaces to be tested and the implementation of such methodologies within a distributed hydrological model. Finally, while normally only events during which soil-slips occurred are used in the calibration of the soil depth distribution, it seems important to also consider all meteorological events during which no instabilities occurred within the basin, to exclude all possible soil depth or parameter distributions that are inconsistent with observations. The assimilation of this progressive information into the calibration process can reduce the margins of uncertainty. Whatever the followed approach, it seems, however, fundamental in future works to recognize the stochastic nature of the soil parameters, e.g., using a Monte Carlo analysis to account for their spatial variability and to assess its importance on the resulting stability maps.

5 | CONCLUSIONS

In many areas of the world, the degree of urbanization of mountain regions is growing, enhancing the hazard caused by soil slips and debris flows. These events cause destruction of properties and claim a significant death toll each year (e.g. Barnhart et al., 2021). Accordingly, in several nations, real-time monitoring and forecast systems are being developed that usually rely on estimated rainfall thresholds for predicting landslides (e.g. Baum & Godt, 2010). Although important, the approach based on rainfall thresholds is purely regressive: it is site-specific and dependent on the available historic record, does not provide any precise indication of the site of possible failure and usually does not take into account the saturation history at the time of landslide occurrence. Finally, it is not capable to deal with changes of the hydrological regime of forested basin, such as the ones caused by uncontrolled forest wildfires, by windthrows (e.g. Mauri & Tarolli, 2023) and by biotic hazards (e.g., Seidl & Rammer, 2017) so that, when applied to a wide territory, it provides a rather vague information about something that could happen somewhere. To be really effective, a forecast system needs something more precise and a physically based hydrological model coupled with a stability model, working with rainfall maps provided either by spatially distributed weather forecast models (e.g., Rojas-Campos et al., 2023) or by radar maps could, in principle, be the appropriate solution. In this work, a slope stability model coupled with a hydrological model to improve the limitations of the IS model has been presented. The proposed model is an improvement of Janbu's method, suitably implemented to catchment scale applications using the drainage network obtained by a DEM. The novel methodology has been validated with an elemental slope using the output of a complete equilibrium analysis as ground truth. In this simple test case, the proposed Janbu's method improved the prediction of the unstable areas provided by the IS model, performing similarly to the complete equilibrium method. Finally, using the well-known Mettman Ridge study case and dataset, it was possible to assess the performance of the two stability models without incurring parameters calibration, an issue which greatly influences the results in any comparison. The Mettman Ridge application shows how the IS model can overestimate the unstable areas, whereas the proposed Janbu's method, by considering on the one hand the actions exchanged between the blocks and on the other hand the lateral contributions, contributes to correct this intrinsic bias of the IS model.

AUTHOR CONTRIBUTIONS

RB and MP conceptualized the work, RB carried out the formal analysis and stability computations. LP supervised geotechnical modeling and MP implemented the hydrological model. All authors contributed to write the paper.

ACKNOWLEDGEMENTS

The permission to use the data set contained in the online repository by Bellugi et al. (2015, 2021), which made it possible to compare the

performance of the proposed model with a real test case, is kindly acknowledged. This paper is part of the Ph. D Thesis of the first author. Open access publishing facilitated by Universita degli Studi di Brescia, as part of the Wiley - CRUI-CARE agreement.

CONFLICT OF INTEREST STATEMENT

The authors declare that they have no conflict of interest.

DATA AVAILABILITY STATEMENT

After the completion of the revision process, the code along with the data set needed to reproduce the first two test cases described in the manuscript will be downloadable from the web page https://hydraulics.unibs.it/hydraulics/dati-scaricabili/, where also a detailed user instruction will be available.

REFERENCES

Arellano, D. & Stark, T.D. (2000) *Importance of three-dimensional slope stability in practice*. Denver, CO: American Society of Civil Engineers, Geo-Denver, pp. 18–32.

Barnhart, K.R., Jones, R.P., George, D.L., McArdell, B.W., Rengers, F.K., Staley, D.M., et al. (2021) Multi-model comparison of computed debris flow runout for the 9 January 2018 Montecito, California post-wildfire event. *Journal of Geophysical Research: Earth Surface*, 126(12), e2021JF006245. Available from: https://doi.org/10.1029/2021JF006245

Baum, R.L. & Godt, J.W. (2010) Early warning of rainfall-induced shallow landslides and debris flows in the USA. *Landslides*, 7(3), 259–272. Available from: https://doi.org/10.1007/s10346-009-0177-0

Baum R.L. Savage W.Z. & Godt J.W. (2008) *TRIGRS – a fortran program for transient rainfall infiltration and grid-based regional slope-stability analysis, version 2.0*. USGS Open-File Report 2008-1159, 75 p. Available from: https://doi.org/10.3133/ofr20081159

Bellugi, D., Milledge, D.G., Cuffey, K.M., Dietrich, W.E. & Larsen, L.G. (2021) Controls on the size distributions of shallow landslides. *Proceedings of the National Academy of Sciences of the United States of America*, 118(9), e2021855118. Available from: https://doi.org/10.1073/pnas.2021855118

Bellugi, D., Milledge, D.G., Dietrich, W.E., McKean, J.A., Perron, J.T., Sudderth, E.B., et al. (2015) A spectral clustering search algorithm for predicting shallow landslide size and location. *Journal of Geophysical Research: Earth Surface*, 120(2), 300–324. Available from: https://doi.org/10.1002/2014JF003137

Bishop, A.W. (1955) The use of the slip circle in the stability analysis of slopes. *Geotechnique*, 5(1), 7–17. Available from: https://doi.org/10.1680/geot.1955.5.1.7

Burroughs, E.R. Jr. (1985) Landslide hazard rating for the Oregon coast range. In: *Proceedings of symposium sponsored by committee on watershed management, irrigation & drainage Div., ASCE*. Denver, CO:ASCE Convention, pp. 132–139.

Casadei, M., Dietrich, W.E. & Miller, N.L. (2003) Testing a model for predicting the timing and location of shallow landslide initiation in soil mantled landscapes. *Earth Surface Processes and Landforms*, 28(9), 925–950. Available from: https://doi.org/10.1002/esp.470

Catani, F., Segoni, S. & Falorni, G. (2010) An empirical geomorphology-based approach to the spatial prediction of soil thickness at catchment scale. *Water Resources Research*, 46(5), 5. Available from: https://doi.org/10.1029/2008WR007450

Chae, B., Lee, J.H., Park, H.J. & Choi, J. (2015) A method for predicting the factor of safety of an infinite slope based on the depth ratio of the wetting front. *Natural Hazards and Earth System Sciences Discussions*, 3, 791–836. Available from: https://doi.org/10.5194/nhessd-3-791-2015

Cheng, Y.M. & Lau, C.K. (2014) *Slope stability analysis and stabilization: new methods and insight*, 2nd edition, CRC Press. https://doi.org/10.1201/b17015

Chicco, D. & Jurman, G. (2023) The Matthews correlation coefficient (MCC) should replace the ROC AUC as the standard metric for assessing binary classification. *Biodata Mining*, 16(1), 4. Available from: https://doi.org/10.1186/s13040-023-00322-4

Cho, S.E. (2017) Prediction of shallow landslide by superficial stability analysis considering rainfall infiltration. *Engineering Geology*, 231, 126–138. Available from: https://doi.org/10.1016/j.enggeo.2017.10.018

Cho, S.E. & Lee, S.R. (2002) Evaluation of surficial stability for homogeneous slopes considering rainfall characteristics. *Journal of Geotechnical and Geoenvironmental Engineering*, 128(9), 756–763. Available from: https://doi.org/10.1061/(ASCE)1090-0241(2002)128:9(756)

Chugh, A.K. (2003) On the boundary conditions in slope stability analysis. *International Journal for Numerical and Analytical Methods in Geomechanics*, 27(11), 905–926. Available from: https://doi.org/10.1002/nag.305

Claessens, L., Heuvelink, G.B.M., Schoorl, J.M. & Veldkamp, A. (2005) DEM resolution effects on shallow landslide hazard and soil redistribution modelling. *Earth Surface Processes and Landforms*, 30(4), 461–477. Available from: https://doi.org/10.1002/esp.1155

Cunge, J.A. (1969) On the subject of a flood propagation computation method (Muskingum method). *Journal of Hydraulic Research*, 7(2), 205–230. Available from: https://doi.org/10.1080/00221686909500264

Davis, J. & Goadrich, M. (2006) The relationship between precision-recall and ROC-curves. In: *Proceedings of the 23rd international conference on Machine learning (ICML '06)*, New York, NY, USA: Association for Computing Machinery, pp. 233–240 https://doi.org/10.1145/1143844.1143874

Dietrich, W.E., Bellugi, D. & Real de Asua, R. (2001) Validation of the shallow landslide model, SHALSTAB, for forest management. In: *Land use and watersheds: human influence on hydrology and geomorphology in urban and Forest areas*, Vol. 2, American Geophysical Union, Water Resources Monograph, pp. 195–227 https://doi.org/10.1029/WS002p0195

Dietrich, W.E., McKean, J., Bellugi, D. & Perron, T. (2008) The prediction of shallow landslide location and size using a multidimensional landslide analysis in a digital terrain model. In: *Proceedings of the fourth international conference on debris-flow hazards mitigation: mechanics, prediction, and assessment (DFHM-4)*. Chengdu, China, The Netherlands, Amsterdam:IOS Press, 12 p.

Dietrich, W.E., Reiss, R., Hsu, M.L. & Montgomery, D.R. (1995) A process-based model for colluvial soil depth and shallow landsliding using digital elevation data. *Hydrological Processes*, 9(3-4), 383–400. Available from: https://doi.org/10.1002/hyp.3360090311

Dietrich, W.E., Wilson, C.J., Montgomery, D.R. & McKean, J. (1993) Analysis of erosion thresholds, channel networks and landscape morphology using a digital terrain model. *Journal of Geology*, 101(2), 259–278. Available from: https://doi.org/10.1086/648220

Dietrich, W.E., Wilson, C.J., Montgomery, D.R., McKean, J. & Bauer, R. (1992) Channelization thresholds and land surface morphology. *Geology*, 20(8), 675–679. Available from: https://doi.org/10.1130/0091-7613(1992)020<0675:ETALSM>2.3.CO;2

Dolojan, N., Moriguchi, S., Hashimoto, M. & Terada, K. (2021) Mapping method of rainfall-induced landslide hazards by infiltration and slope stability analysis. *Landslides*, 18(6), 2039–2057. Available from: https://doi.org/10.1007/s10346-020-01617-x

Gabet, E.J. & Dunne, T. (2002) Landslides on coastal sage-scrub and grassland hillslopes in a severe El Nino winter: the effects of vegetation conversion on sediment delivery. *Geological Society of America Bulletin*, 114(8), 983–990. Available from: https://doi.org/10.1130/0016-7606(2002)114<0983:LOCSSA>2.0.CO;2

GeoStudio. (2021). Stability Modeling with GeoStudio. GeoStudio Documentation, Online. Available from: https://files.seequent.com/GeoStudio/Manuals/Slope%20Stability%20Modeling.pdf

Green, W.H. & Ampt, G.A. (1911) Studies on soil physics. *Journal of Agricultural Science*, 4(1), 1–24. Available from: https://doi.org/10.1017/S0021859600001441

Griffiths, D.V., Huang, J. & deWolfe, G.F. (2011) Numerical and analytical observations on long and infinite slopes. *International Journal for*

Numerical and Analytical Methods in Geomechanics, 35(5), 569–585. Available from: https://doi.org/10.1002/nag.909

Guzzetti, F., Gariano, S.L., Peruccacci, S., Brunetti, M.T., Marchesini, I., Rossi, M., et al. (2020) Geographical landslide early warning systems. *Earth-Science Reviews*, 200, 102973. Available from: https://doi.org/10.1016/j.earscirev.2019.102973

Haefeli, R. (1948) The stability of slopes acted upon by parallel seepage. In:*Proc. 2nd Int. Conf. on Soil Mechanics and Foundation Engineering* , Vol. 1, Rotterdam, Netherlands: Municipality of Rotterdam, pp. 57–62.

Hovland, H.J. (1977) Three-dimensional slope stability analysis method. *ASCE Journal of the Geotechnical Engineering Division*, 103(GT9), 971–986. Available from: https://doi.org/10.1061/AJGEB6.0000493

Hungr, O., Salgado, F.M. & Byrne, P.M. (1989) Evaluation of a three-dimensional method of slope stability analysis. *Canadian Geotechnical Journal*, 26(4), 679–686. Available from: https://doi.org/10.1139/t89-079

Iida, T. (2004) Theoretical research on the relationship between return period of rainfall and shallow landslides. *Hydrological Processes*, 18(4), 739–756. Available from: https://doi.org/10.1002/hyp.1264

Iverson, R.M. (2000) Landslide triggering by rain infiltration. *Water Resources Research*, 36(7), 1897–1910. Available from: https://doi.org/10.1029/2000WR900090

Janbu, N. (1973) Slope stability computations. In: Hirschfeld, R.C. & Poulos, S.J. (Eds.) *Embankment dam engineering, Casagrande volume*. New York: John Wiley and Sons, pp. 47–86.

Lehmann, P. & Or, D. (2012) Hydromechanical triggering of landslides: from progressive local failures to mass release. *Water Resources Research*, 48(3), 2011WR010947. Available from: https://doi.org/10.1029/2011WR010947

Manning, C.D. & Schutze, H. (1999) *Foundations of statistical natural language processing*. Cambridge, MA: MIT Press.

Mauri, L. & Tarolli, P. (2023) Modeling windthrow effects on water runoff and hillslope stability in a mountain catchment affected by the VAIA storm. *Science of the Total Environment*, 895, 164831. Available from: https://doi.org/10.1016/j.scitotenv.2023.164831

Medina, V., Hürlimann, M., Guo, Z., Lloret, A. & Vaunat, J. (2021) Fast physically-based model for rainfall-induced landslide susceptibility assessment at regional scale. *Catena*, 201, 105213. Available from: https://doi.org/10.1016/j.catena.2021.105213

Metz, C.E. (1978) Basic principles of ROC analysis. *Seminars in Nuclear Medicine*, 8(4), 283–298. Available from: https://doi.org/10.1016/S0001-2998(78)80014-2

Milledge, D.G., Griffiths, D., Lane, S.N. & Warburton, J. (2012) Limits on the validity of infinite length assumptions for modelling shallow landslides. *Earth Surface Processes and Landforms*, 37(11), 1158–1166. Available from: https://doi.org/10.1002/esp.3235

Montgomery, D.R. & Dietrich, W.E. (1994) A physically based model for the topographic control on shallow landsliding. *Water Resources Research*, 30(4), 1153–1171. Available from: https://doi.org/10.1029/93WR02979

Montgomery, D.R., Schmidt, K.M., Dietrich, W.E. & Greenberg, H.M. (2000) Forest clearing and regional landsliding in the Pacific northwest. *Geology*, 28(4), 311–314. Available from: https://doi.org/10.1130/0091-7613(2000)28<311:FCARL>2.0.CO;2

Montrasio, L., Valentino, R. & Losi, G.L. (2011) Towards a real-time assessment of rainfall induced shallow landslides on a regional scale. *Natural Hazards and Earth System Sciences*, 11(7), 1927–1947. Available from: https://doi.org/10.5194/nhess-11-1927-2011

Morgenstern, N.R. & Price, V.E. (1965) The analysis of the stability of general slip surfaces. *Geotechnique*, 15(1), 79–93. Available from: https://doi.org/10.1680/geot.1965.15.1.79

Murgia, I., Giadrossich, F., Mao, Z., Cohen, D., Capra, G.F. & Schwarz, M. (2022) Modeling shallow landslides and root reinforcement: a review. *Ecological Engineering*, 181, 106671. Available from: https://doi.org/10.1016/j.ecoleng.2022.106671

Oguz, E.A., Depina, I. & Thakur, V. (2022) Effects of soil heterogeneity on susceptibility of shallow landslides. *Landslides*, 19(1), 67–83. Available from: https://doi.org/10.1007/s10346-021-01738-x

Okimura, T. (1994) Prediction of the shape of a shallow failure on a mountain slope: the three-dimensional multi-planar sliding surface method. *Geomorphology*, 9(3), 223–233. Available from: https://doi.org/10.1016/0169-555X(94)90064-7

Piciullo, L., Calvello, M. & Cepeda, J. (2018) Territorial early warning systems for rainfall-induced landslides. *Earth-Science Reviews*, 179, 228–247. Available from: https://doi.org/10.1016/j.earscirev.2018.02.013

Pilotti, M., Chapra, S.C. & Valerio, G. (2019) Steady-state distributed modeling of dissolved oxygen in data-poor, sewage dominated river systems using drainage networks. *Environmental Modelling & Software*, 111, 153–169. Available from: https://doi.org/10.1016/j.envsoft.2018.08.027

Pilotti, M., Gandolfi, C. & Bischetti, G.B. (1996) Identification and analysis of natural channel networks from digital elevation models. *Earth Surface Processes and Landforms*, 21(11), 1007–1020. Available from: https://doi.org/10.1002/(SICI)1096-9837(199611)21:11<1007::AID-ESP704>3.0.CO;2-V

Pilotti, M. & Rosso, R. (1990) Shell: a general framework for modeling the distributed response of a drainage basin. In: *Computational methods in surface hydrology*. Berlin: Springer Verlag, pp. 517–522.

Qi, S., Ling, D., Yao, Q., Lu, G., Yang, X. & Zhou, J. (2021) Evaluating slope stability with 3D limit equilibrium technique and its application to landfill in China. *Engineering Geology*, 280, 105939. Available from: https://doi.org/10.1016/j.enggeo.2020.105939

Qiu, C.T., Esaki, T., Kie, M., Mitani, Y. & Wang, C. (2007) Spatio-temporal estimation of shallow landslide hazard triggered by rainfall using a three-dimensional model. *Environmental Geology*, 52(8), 1569–1579. Available from: https://doi.org/10.1007/s00254-006-0601-x

Reid M.E. Christian S.B. Brien D.L. Henderson S.T. 2015 Scoops3d—software to analyze three-dimensional slope stability throughout a digital landscape; US Geological Survey Techniques and Methods, p. 218

Rojas-Campos, A., Langguth, M., Wittenbrink, M. & Pipa, G. (2023) Deep learning models for generation of precipitation maps based on numerical weather prediction. *Geoscientific Model Development*, 16(5), 1467–1480. Available from: https://doi.org/10.5194/gmd-16-1467-2023

Rossi, G., Catani, F., Leoni, L., Segoni, S. & Tofani, V. (2013) HIRESSS: a physically based slope stability simulator for HPC applications. *Natural Hazards and Earth System Sciences*, 13(1), 151–166. Available from: https://doi.org/10.5194/nhess-13-151-2013

Rosso, R., Rulli, M.C. & Vannucchi, G. (2006) A physically based model for the hydrologic control on shallow landsliding. *Water Resources Research*, 42(6), W06410, Available from: https://doi.org/10.1029/2005WR004369

Sannino, G., Tomei, F., Bittelli, M., Bordoni, M., Meisina, C. & Valentino, R. (2024) Implementation of a slope stability method in the CRITERIA-1D agro-hydrological modeling scheme. *Landslides*, 21(11), 2597–2616. Available from: https://doi.org/10.1007/s10346-024-02313-w

Schwanghart, W. & Kuhn, N.K. (2010) Topotoolbox: a set of Matlab functions for topographic analysis. *Environmental Modelling & Software*, 25(6), 770–781, Available from: https://doi.org/10.1016/j.envsoft.2009.12.002

Seidl, R. & Rammer, W. (2017) Climate change amplifies the interactions between wind and bark beetle disturbances in forest landscapes. *Landscape Ecology*, 32(7), 1485–1498. Available from: https://doi.org/10.1007/s10980-016-0396-4

Skempton, A.W. & DeLory, F.A. (1957) Stability of natural slopes in London clay. In: *4th international conference on soil mechanics and foundation engineering*, London: Thomas Telford Publishing, pp. 378–381. Available from: https://doi.org/10.1680/sposm.02050.0011

Spencer, E. (1967) A method of analysis of the stability of embankments assuming parallel interslice forces. *Geotechnique*, 17(1), 11–26. Available from: https://doi.org/10.1680/geot.1967.17.1.11

Taylor, D.W. (1948) *Fundamentals of soil mechanics*. New York: Wiley.

U.S. Army Corps of Engineers. (2003) *Slope Stability, Engineering and Design*. EM 1110-2-1902. Washington , DC: U.S. Army Corps of Engineers.

Xie, M., Esaki, T. & Cai, M. (2004) A time-space based approach for mapping rainfall-induced shallow landslide hazard. *Environmental Geology*, 46(6-7), 840–850. Available from: https://doi.org/10.1007/s00254-004-1069-1

SUPPORTING INFORMATION

Additional supporting information can be found online in the Supporting Information section at the end of this article.

How to cite this article: Bonomelli, R., Pilotti, M. & Piciullo, L. (2025) A novel approach for the computation of soil slope stability in distributed hydrologic applications. *Earth Surface Processes and Landforms*, 50(9), e70122. Available from: https://doi.org/10.1002/esp.70122